nature medicine

Genetic and acute CPEB1 depletion ameliorate fragile X pathophysiology

Tsuyoshi Udagawa[1,8,9], Natalie G Farny[1,9], Mira Jakovcevski[2,8,9], Hanoch Kaphzan[3,8], Juan Marcos Alarcon[4], Shobha Anilkumar[5], Maria Ivshina[1], Jessica A Hurt[6], Kentaro Nagaoka[1,8], Vijayalaxmi C Nalavadi[7], Lori J Lorenz[1], Gary J Bassell[7], Schahram Akbarian[2,8], Sumantra Chattarji[5], Eric Klann[3] & Joel D Richter[1]

Fragile X syndrome (FXS), the most common cause of inherited mental retardation and autism, is caused by transcriptional silencing of *FMR1*, which encodes the translational repressor fragile X mental retardation protein (FMRP). FMRP and cytoplasmic polyadenylation element–binding protein (CPEB), an activator of translation, are present in neuronal dendrites, are predicted to bind many of the same mRNAs and may mediate a translational homeostasis that, when imbalanced, results in FXS. Consistent with this possibility, *Fmr1*$^{-/y}$; *Cpeb1*$^{-/-}$ double-knockout mice displayed amelioration of biochemical, morphological, electrophysiological and behavioral phenotypes associated with FXS. Acute depletion of CPEB1 in the hippocampus of adult *Fmr1*$^{-/y}$ mice rescued working memory deficits, demonstrating reversal of this FXS phenotype. Finally, we find that FMRP and CPEB1 balance translation at the level of polypeptide elongation. Our results suggest that disruption of translational homeostasis is causal for FXS and that the maintenance of this homeostasis by FMRP and CPEB1 is necessary for normal neurologic function.

FXS, the most common inherited form of mental retardation and syndromic autism[1,2], is caused by inactivation of the *FMR1* gene[3]. FXS phenotypes include cognitive dysfunction, repetitive behaviors, anxiety, seizures and morphological abnormalities[1]. *Fmr1* encodes FMRP, a widely expressed RNA-binding protein that is found in neuronal soma and synaptodendrites[4]. FMRP binds target mRNAs predominantly in coding regions and probably represses translation by tempering transit of polypeptide-elongating ribosomes[5]. It responds to signaling from group I metabotropic glutamate receptors (mGluRs)[6,7], which mediate its translation-repressing activity[8]. In *Fmr1*$^{-/y}$ (*Fmr1* KO) (because *Fmr1* is on the X chromosome, hemizygotes lack this gene on the Y chromosome and are denoted as *Fmr1*$^{-/y}$) mice, protein synthesis is elevated by ~20% (refs. 7,9–11), which is probably responsible for the synapse dysmorphogenesis, aberrant synaptic plasticity[7,12] and behavioral and cognitive dysfunctions displayed by children with FXS and animal models of the disease. FMRP binds >1,000 mRNAs in the brain[5], and determining which contribute to FXS pathophysiology is a daunting task.

CPEB1 also affects synapse function[13–16]; it binds the 3′ untranslated region (UTR) cytoplasmic polyadenylation element (CPE) of target mRNAs and stimulates polyadenylation-induced translation[13,17]. In neurons, CPEB is localized to synaptodendrites[13,18] and activates translation in response to synaptic stimulation[17,18]. *Cpeb1*$^{-/-}$ (*Cpeb1* KO) mice show neurological phenotypes including perseverative hippocampal-dependent memory[19] and defects in long-term potentiation[15], underscoring the importance of CPEB in regulating translation and neural function.

We hypothesized that the translational imbalance and associated pathophysiologies in FXS mice such as audiogenic seizure and learning and memory impairments might be rescued if the loss of FMRP were accompanied by ablation of a factor that stimulates rather than represses translation. In the normal condition, translation could be balanced by FMRP and this unknown factor; unbalanced translation due to the loss of FMRP causes FXS, but perhaps ablation of the counter-balancing factor could rebalance translation and restore normal neurologic function (**Supplementary Fig. 1a**). We surmised that the unknown factor could be CPEB1 because about one-third of FMRP-bound mRNAs[5] contain 3′ UTR CPEs, and thus they are potential targets for CPEB1 (**Supplementary Fig. 2b** and **Supplementary Table 1**). Indeed, several mRNAs immunoprecipitate with both FMRP and CPEB1 (**Fig. 1a**). Moreover, CPEB1 and FMRP colocalize in dendrites of cultured hippocampal neurons (**Supplementary Fig. 2a**,**b**) and co-purify in cultured neuroblastoma cells and a cell-free system (**Supplementary Fig. 2c**–**f**). Consequently, we generated *Fmr1*$^{-/y}$; *Cpeb1*$^{-/-}$ double-knockout (DKO) mice (**Supplementary Fig. 3**) and examined protein synthesis in them. Although *Fmr1* KO animals had ~15% more protein synthesis in acute hippocampal slices compared to wild-type (WT) mice, protein synthesis in DKO mice was similar to that in WT (**Fig. 1b**), suggesting that translational homeostasis was restored in these animals. There was no significant decrease in protein synthesis in the *Cpeb1* KO animals.

[1]Program in Molecular Medicine, University of Massachusetts Medical School, Worcester, Massachusetts, USA. [2]Department of Psychiatry, Brudnik Neuropsychiatric Research Institute, University of Massachusetts Medical School, Worcester, Massachusetts, USA. [3]Center for Neural Science, New York University, New York, New York, USA. [4]Department of Pathology, State University of New York, Downstate Medical Center, Brooklyn, New York, USA. [5]Center for Brain Development and Repair, The Institute for Stem Cell Biology and Regenerative Medicine and National Center for Biological Sciences, Bangalore, India. [6]Department of Biology, Massachusetts Institute of Technology, Cambridge, Massachusetts, USA. [7]Department of Cell Biology, Emory University School of Medicine, Atlanta, Georgia, USA. [8]Present addresses: Department of Neurology, Nagoya University School of Medicine, Nagoya, Japan (T.U.), Max Planck Institute of Psychiatry, Munich, Germany (M.J.), Laboratory for Neurobiology of Psychiatric Disorders, Sagol Department of Neurobiology, University of Haifa, Mount Carmel, Haifa, Israel (H.K.), Department of Veterinary Medicine, Tokyo University of Agriculture and Technology, Tokyo, Japan (K.N.), and Friedman Brain Institute, Departments of Psychiatry and Neuroscience, Icahn School of Medicine at Mount Sinai, New York, New York, USA (S.A.). [9]These authors contributed equally to this work. Correspondence should be addressed to J.D.R. (joel.richter@umassmed.edu).

Received 17 May; accepted 20 August; published online 20 October 2013; doi:10.1038/nm.3353

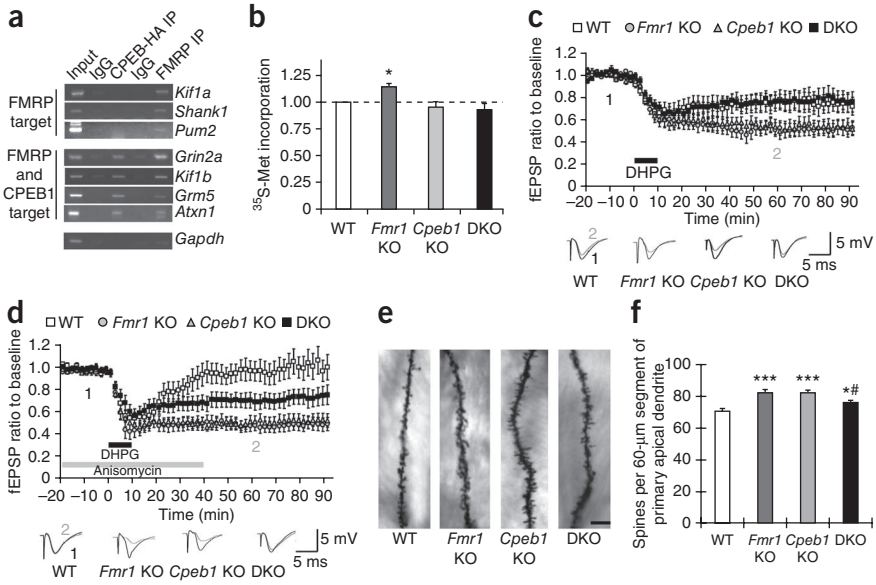

Figure 1 Interplay between FMRP and CPEB1 in the brain. (**a**) Co-immunoprecipitation (IP) of RNAs with FMRP or epitope-tagged CPEB1 from neurons. IgG served as a negative control. *Kif1a*, kinesin family member 1A; *Shank1*, SH3 and multiple ankyrin repeat domains 1; *Pum2*, pumilio 2; *Grin2a*, glutamate receptor, ionotropic, NMDA2A; *Grm5*, glutamate receptor, metabotropic 5; *Atxn1*, ataxin 1; *Gapdh*, glyceraldehyde-3-phosphate dehydrogenase. (**b**) Acute hippocampal slices were labeled with [^{35}S]methionine, and incorporation into protein was determined by scintillation counting ($n = 4$; analysis of variance (ANOVA), $F_{(3,12)} = 5.458$, $P < 0.05$). $^{*}P < 0.05$ as compared to wild-type (Student's *t*-test). Error bars are s.e.m. (**c**) DHPG-induced LTD at Schaffer collateral-CA1 synapses measured in the *Fmr1* KO ($n = 15$, repeated measures (RM)-ANOVA, $P < 0.001$) and *Cpeb1* KO ($n = 19$, RM-ANOVA, $P < 0.001$) hippocampal slices were compared to WT slices ($n = 12$). The DHPG-induced LTD in the DKO slices was also compared to WT slices ($n = 14$, RM-ANOVA, $P > 0.05$). fEPSP, excitatory postsynaptic potential. (**d**) DHPG-induced LTD measured in hippocampal slices treated with either vehicle (data from **c**) or anisomycin for each genotype (WT, $n = 13$, RM-ANOVA, $P < 0.001$; comparisons of other genotypes were not statistically significant, $P > 0.05$, RM-ANOVA). DHPG-induced LTD in the DKO slices treated with anisomycin was also compared with the LTD observed in *Fmr1* KO, *Cpeb1* KO, and WT slices that were also treated with anisomycin (RM-ANOVA, $P < 0.001$ for each comparison). (**e**) Representative images of Golgi-Cox–stained dendritic segments of CA1 pyramidal neurons of the hippocampus from WT, *Fmr1* KO, *Cpeb1* KO and DKO mice. Scale bar, 20 µm. (**f**) Total number of spines quantified along a 60-µm segment from the origin of primary apical dendritic branches of Golgi-Cox–stained CA1 pyramidal neurons. $n = 26$ dendritic segments, $^{***}P < 0.001$, $^{*}P < 0.05$, as compared to WT (ANOVA). $^{\#}P < 0.05$ by two-way ANOVA (*Fmr1* KO versus DKO). Error bars are s.e.m.

We examined the levels of specific proteins in hippocampal lysates from mice of all four genotypes (**Supplementary Table 2**). The amounts of several proteins encoded by FMRP target mRNAs were increased in *Fmr1* KO animals compared to WT animals. Consistent with previous reports of CPEB1 function, translation of many mRNAs was decreased in *Cpeb1* KO animals compared to WT mice. In DKO animals, translation of FMRP targets was either similar to that in WT mice or decreased as observed in the *Cpeb1* KO hippocampus. These results suggest that in DKO animals a 'brake' is placed on the runaway translation observed in the *Fmr1* KO brain. We also examined specific protein levels by western blot analysis of cortical samples, but we found few significant differences between WT and *Fmr1* KO animals (**Supplementary Table 3**).

Because previous studies noted an increase in mammalian target of rapamycin and extracellular signal–regulated kinase 1 and 2 signaling in *Fmr1* KO animals[9,11], we examined the phosphorylation states and relative levels of several components of these signaling pathways. We did not observe a consistent pattern of enhanced signaling through either pathway. (**Supplementary Table 2**) P70 ribosomal S6 kinase 1 (S6K1) lies downstream of both the extracellular signal–regulated kinase and mammalian target of rapamycin pathways, and although its phosphorylation was not significantly altered, phosphorylation of its immediate downstream target, ribosomal protein S6, was significantly increased in the *Fmr1* KO hippocampus. (**Supplementary Table 2**; see also ref. 9). The levels of phospho-S6 were similar in *Cpeb1* KO and DKO animals, (**Supplementary Table 2**) indicating that signaling through S6K1 is restored in DKO animals. By analyzing the levels of specific proteins (**Supplementary Table 2**) as well as general protein synthesis (**Fig. 1b**), we demonstrate that CPEB and FMRP balance translation in the brain.

mGluRs are hyperactivated in *Fmr1* KO mice, as evidenced by enhanced mGluR-dependent long-term depression (LTD) at Schaffer collateral-CA1 synapses in the hippocampus[7,12,20]. *Fmr1* KO and *Cpeb1* KO mice have both displayed exaggerated LTD in hippocampal slices treated with dihydroxyphenylglycine (DHPG) (**Fig. 1c**), a group I mGluR agonist[12]. LTD was at WT levels in slices derived from DKO animals (**Fig. 1c**). Basal synaptic transmission and presynaptic function were not affected in the DKO animals (**Supplementary Fig. 4a**,**b**). Because DHPG-induced LTD is a translation-dependent process[12], we determined whether application of the protein synthesis inhibitor anisomycin attenuated LTD in hippocampal slices. Anisomycin inhibited LTD in WT slices but had no effect on *Fmr1* KO, *Cpeb1* KO or DKO slices (**Fig. 1d**). These results suggest that the protein synthesis dependency in the DKO slices occurs before mGluR stimulation, perhaps during synapse formation.

Long-term potentiation (LTP) is also affected in the *Fmr1* KO hippocampus under certain stimulation protocols[21]. We previously reported a deficit in LTP induced by theta burst stimulation (TBS-LTP) in *Cpeb1* KO mice[15,16]. We therefore examined TBS-LTP in *Fmr1* KO and DKO animals. Although *Fmr1* KO animals displayed normal TBS-LTP, DKO animals also displayed normal TBS-LTP (**Supplementary Fig. 4c**–**e**), suggesting the deficit in TBS-LTP previously seen in *Cpeb1* KO animals is rescued by the absence of FMRP. However, when we induced LTP with 1 mM glycine (Gly-LTP), which requires mGluR receptor function[21], *Fmr1* KO animals showed a deficit compared to WT animals, which was again rescued in the DKO (**Supplementary Fig. 4d**). Therefore, both LTP and LTD defects in synaptic plasticity in the *Fmr1* KO hippocampus seem to be largely dependent upon mGluR signaling and are both rescued in DKO animals.

Dendritic spine density, which is commonly increased in FXS[7,9], was enhanced *in vivo* in both *Fmr1* KO and *Cpeb1* KO mice on the primary apical dendritic branches of hippocampal CA1 pyramidal neurons (**Fig. 1e**,**f** and **Supplementary Fig. 5a**,**b**). Spine density was reduced in the DKO neurons, demonstrating that FMRP and CPEB1 balance one

another to control synapse number (**Fig. 1e**,**f**). We further compared synapse formation in hippocampal and cortical neuron cultures[22] and found in both cases that an increase in synaptic puncta in *Fmr1* KO neurons was partially restored in DKO neurons (**Supplementary Fig. 6a–d**). Total body weight, which is increased in adolescent *Fmr1* KO animals, was reversed to WT level in DKO animals (**Supplementary Fig. 5c**), suggesting that the interplay between FMRP and CPEB1 that leads to phenotypic rescue is not limited to the brain.

To examine whether higher neural function is rescued in the DKO mice, we tested animals for their sensitivity to acoustic stimulation, which in *Fmr1* KO mice results in an initial period of wild running followed by tonic-clonic seizures, status epilepticus and, in some cases, death[7,11]. WT and *Cpeb1* KO animals were little affected by the acoustic stimulus, but the *Fmr1* KO mice displayed the expected running and seizure responses (**Fig. 2a**). The seizure phenotype was reduced by ~50% in the DKO animals as well as in $Fmr1^{-/y}$; $Cpeb1^{+/-}$ heterozygous (HKO) animals (**Fig. 2a**).

Fmr1 KO mice displayed decreased anxiety as suggested by their tendency to remain in the center of an open experimental field 45% longer than WT animals, which preferentially moved about the periphery[23] (**Fig. 2b**). *Cpeb1* KO animals were comparable to WT mice with respect to time in the center field, although they moved slightly less than WT mice (**Supplementary Fig. 7a**). The DKO animals were indistinguishable from WT mice for time in the center and distance moved. Reducing the CPEB1 dose by one-half (HKO) in heterozygous animals did not ameliorate the anxiety phenotype (**Fig. 2b**).

We examined learning and memory by assessing passive avoidance. Mice placed into a light chamber of a two-chamber test apparatus readily moved to the dark chamber where a foot shock was administered. After 24 h, the test was repeated, and in all genotypes there was increased latency in entering the dark chamber, indicating memory of the foot shock (**Fig. 2c**). Although we did not observe a statistical difference in the learning ability between WT and *Fmr1* KO

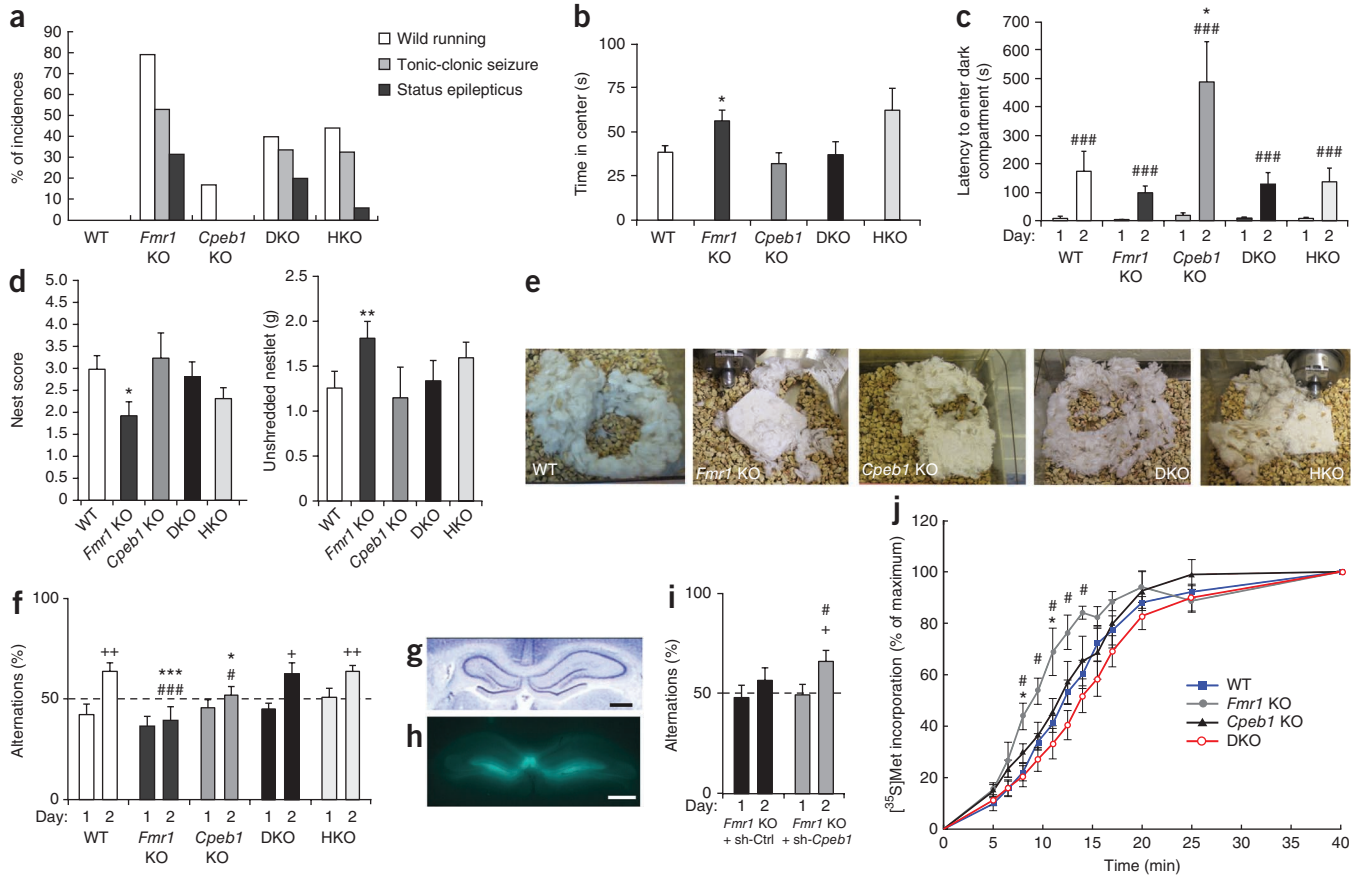

Figure 2 *Cpeb1* deletion ameliorates FXS-related behavioral abnormalities. (**a**) Audiogenic seizure in WT ($n = 6$), *Fmr1* KO ($n = 19$), *Cpeb1* KO ($n = 6$), DKO ($n = 15$) and *Fmr1* KO/*Cpeb1* heterozygous (HKO) ($n = 34$) mice at postnatal days 19–21. Seizure reduction in the DKO (40%) and HKO (44%) compared to *Fmr1* KO was significant (79%, $P < 0.05$, Fisher's exact test). (**b**) Time spent in the center of an open field for 15 min ($n = 9$–11, ANOVA, $F_{(4,46)} = 3.28$, $P < 0.05$). (**c**) Passive avoidance memory measured by latency to enter a dark compartment 24 h after foot shock in the dark ($n = 8$–11; ANOVA on effect of day $F_{(1,44)} = 43.5$ and $P < 0.001$, on genotype $F_{(4,44)} = 5.04$ and $P < 0.01$). (**d**) Nest building scored on a scale of 1–5 (ref. 31) (left) and weight of unused nesting 24 h after 2.5 g nestlet presentation ($n = 9$–18, ANOVA, $F_{(4,70)} = 2.93$, $P = 0.058$ and $F_{(4,70)} = 1.63$, $P = 0.17$, respectively) (right). (**e**) Nests after 72 h. (**f**) T maze assay of spontaneous alternations ($n = 8$–11, ANOVA on genotype $F_{(4,44)} = 4.48$, $P < 0.01$). (**g**) H&E-stained hippocampus. Scale bar, 1 mm. (**h**) Hippocampus after bilateral injection with GFP/shRNA-expressing lentivirus. Scale bar, 1 mm. (**i**) T maze assay after bilateral hippocampal injection of *Fmr1* KO mice with lentivirus expressing sh-Ctrl or sh-*Cpeb1* ($n = 8$–11 per treatment per genotype). (**j**) Ribosome transit rate in brain lysates. Quantification of radiolabel incorporation was plotted as a percentage of the maximum (40 min). WT versus *Fmr1* KO, $^{*}P < 0.05$; *Fmr1* KO versus DKO, $^{\#}P < 0.05$ (ANOVA, followed by Bonferroni's *post hoc* test, $n = 3$ or 4 per genotype; **Supplementary Table 5**). For all panels, $^{*}P < 0.05$ and $^{**}P < 0.01$ compared to WT (Mann-Whitney *U* test); $^{\#}P < 0.05$ and $^{\#\#\#}P < 0.001$ compared to performance on day 1 (paired *t* test); $^{+}P < 0.05$ and $^{++}P < 0.01$ (Wilcoxon signed-rank test to test the difference from chance level of 50%). Error bars are s.e.m.

animals, the *Cpeb1* KO animals displayed increased latency of moving to the dark field, indicative of enhanced learning (**Fig. 2c**). This exaggerated learning was restored to WT levels in the DKO mice, demonstrating that the loss of FMRP corrected for the loss of CPEB1. These results support the hypothesis that FMRP and CPEB1 maintain a functional homeostasis in the brain that is critical for normal cognition. We observed normal circadian activity for all genotypes (**Supplementary Fig. 7b**).

Nest building is a social behavior in mice that is affected in another model of syndromic autism[24]. We gave the animals squares of pressed cotton nesting material (nestlet) and scored them 24 and 72 h later for shape and amount of unused nestlet. At 24 h, nest quality of *Fmr1* KO animals was poorer than that of WT mice (**Fig. 2d**). The *Fmr1* KO mice also used less material in nest construction (**Fig. 2d**,**e**). The nest quality and nestlet usage of both *Cpeb1* KO and DKO animals were not distinguishable from those of WT mice. The differences in nest quality among the four genotypes did not reflect time required for construction, as we observed similar results after 72 h (**Supplementary Fig. 7c**,**d**). Therefore, this autism-related paradigm is rescued by simultaneous depletion of FMRP and CPEB1.

We examined spatial working memory using a T-maze assay. We placed animals in the start arm of a T-shaped maze and allowed them to explore. Upon reaching the junction of the T arms, the animal must move right or left. Once the choice of direction was made, access to the non-chosen arm was denied by a door until the animal returned on its own to the start arm. The door was then reopened and the paradigm repeated until the animal made 15 choices. WT mice chose right or left arms randomly on day 1 but chose alternating arms on day 2, which suggests they were aware of which arm they had most recently visited, a characteristic of working memory known as spontaneous alternation (SA) (**Fig. 2f**). Both *Fmr1* KO and *Cpeb1* KO animals had deficient SA on day 2; the DKO and HKO animals, however, displayed SA indistinguishable from WT, indicating a rescue of working memory (**Fig. 2f**). Working memory is thought to involve the hippocampus, particularly in adolescent mice[25,26]. To determine whether acute depletion of CPEB1 could rescue working memory, we injected lentivirus encoding GFP and shRNA targeting *Cpeb1* (sh-Cpeb), or a nontargeting control (sh-Ctrl), bilaterally into the hippocampi of 30-d-old *Fmr1* KO animals (**Fig. 2g**,**h**). After allowing for efficient depletion (**Supplementary Fig. 7e**,**f**), we tested injected animals in the T maze. Sh-Ctrl–injected *Fmr1* KO animals displayed SA on day 2 that was not statistically distinct from random chance (50%) (**Fig. 2i**). Notably, sh-Cpeb–injected *Fmr1* KO animals demonstrated improvement in SA on day 2 compared to the random chance level (**Fig. 2i**), indicating improvement in working memory upon acute depletion of CPEB.

FMRP predominantly binds the coding regions of mRNAs and may slow the translocation of ribosomes during polypeptide elongation[5,27]. In the absence of FMRP, ribosomes can translocate unimpeded and will produce more polypeptide from target mRNAs (**Supplementary Fig. 8a**). Because general and specific protein synthesis is restored in DKO animals (**Fig. 1b** and **Supplementary Table 2**), we wanted to determine whether this rescue could be attributed to a restoration of ribosome translocation rate. We employed an assay to monitor the ribosome transit rate (RTR) in brain lysates (without the cerebellum and midbrain) that is based on the run-off of ribosomes that are actively engaged in translation[5]. We added both [^{35}S]methionine and [^{35}S]cysteine to lysates from the four genotypes and allowed the ribosomes to elongate polypeptides without new initiation (**Supplementary Fig. 8b**, ref. 7). When all active ribosomes have completed their elongation phase, the radioactive signal reaches saturation, which corresponds to the RTR[28]. Our results show that brain extracts derived from *Fmr1* KO mice have an enhanced RTR compared to those from WT mice (**Fig. 2j** and **Supplementary Table 4**). The RTRs in *Cpeb1* KO and DKO samples were indistinguishable from those of WT mice, demonstrating complete restoration of polypeptide elongation rate. These results identify the polypeptide elongation machinery as being essential for the translational homeostasis maintained by FMRP and CPEB1 in the brain.

Brain-associated FXS pathophysiologies are probably caused by excessive translation in neurons[2,7,9,11], which may also occur in syndromic and idiopathic forms of autism[29,30]. We have restored the translational landscape that is altered in FXS by genetically ablating CPEB1, which we surmised acts as an mRNA-specific translational counterweight to FMRP in the brain. When coupled to the loss of FMRP, the additional loss of CPEB restores several biochemical, morphological, electrophysiological and behavioral phenotypes associated with FXS (**Supplementary Table 5**). Furthermore, our data, which confirm and extend the observations of several laboratories[5,27] indicating that FMRP inhibits polypeptide elongation, demonstrate that ribosome transit times are excessive in FMRP KO brains but are mitigated with the concomitant loss of CPEB1. This targeting of the ribosome transit machinery by FMRP and CPEB1 suggests that our original hypothesis, that the two act to balance mRNA-specific translation to maintain normal neural function, requires modification. Although these two proteins could act on common mRNAs that mediate polypeptide elongation, such as eEF2 (**Supplementary Table 2**), they might also regulate distinct components to maintain elongation equilibrium. Indeed, one issue arising from our study is how the loss of CPEB1, which alone has no detectable effect on ribosome transit, palliates this process upon loss of FMRP. Cytoplasmic polyadenylation-induced translation is a main CPEB1 activity that could regulate an elongation 'sensor' involved in restoring protein synthesis (**Supplementary Fig. 8c**).

Because the *Fmr1* KO and *Cpeb1* KO mice display enhanced DHPG-induced LTD, it is not intuitively obvious how this measure of synaptic efficacy is rescued in the DKO mice. FMRP and CPEB1 are both downstream of group I mGluRs because the KO of each has a deficient response to DHPG treatment. These proteins are unlikely to be completely epistatic to one another and could reside at least partially in different regulatory pathways, such that biologic responses to null mutations in each gene could be cancelled by null mutations in both genes. If such pathways include positive and negative influences on LTD, then one could envision how two wrongs (for example, immature dendritic spines) make a right (i.e., near WT spines in the DKO mice).

We rescued working memory, an FXS-associated pathology in adult *Fmr1* KO mice, by injecting lentivirus expressing shRNA for CPEB1 bilaterally into the hippocampus. Working memory requires the hippocampus as well as the prefrontal cortex but is generally thought to be independent of protein synthesis[26]. Although protein synthesis is not required for the short working memory time (several minutes), the CPEB1 shRNA was injected 10 d before the memory test, sufficient time for it to alter translation homeostasis. These experiments demonstrate that at least this one characteristic of FXS, which is generally thought to be a developmental disease, can be reversed in the adult. Therefore, therapies that target CPEB1 and/or the translational apparatus, particularly the polypeptide elongation machinery, might be efficacious in ameliorating other features of FXS.

METHODS

Methods and any associated references are available in the online version of the paper.

Note: Any Supplementary Information and Source Data files are available in the online version of the paper.

ACKNOWLEDGMENTS

We thank N. Dawra for technical assistance, P. Lombroso (Yale University) and C. Proud (University of Southampton) for kind gifts of antibodies (STEP and eEF2, respectively), J. Pelletier (McGill University) for the kind gift of hippuristanol and members of the Richter lab for helpful discussions. T.U. and N.G.F. gratefully acknowledge fellowships from the FRAXA Research Foundation. J.A.H. was supported by US National Institutes of Health NRSA Postdoctoral Fellowship F32GM095060. This work was supported by NIH grants GM46779 and NS079415 to J.D.R. and MH086509 to S. Akbarian.

AUTHOR CONTRIBUTIONS

T.U. and J.D.R. conceived of the initial project with much input from L.J.L. T.U., N.G.F. and M.J. designed and performed the majority of the experiments. H.K. and E.K. performed the electrophysiology experiments in **Figure 1c**,**d** and **Supplementary Figure 4a**,**b**. J.M.A. performed the electrophysiology experiments in **Supplementary Figure 4c**–**e**. S. Anilkumar and S.C. performed spine density analysis in **Figure 1e**,**f** and **Supplementary Figure 5a**,**b**. M.I. created and tested the CPEB antibody used in **Supplementary Figure 2f**. J.A.H. performed the bioinformatics analysis in **Supplementary Table 1**. V.C.N. and G.J.B. performed the immunocytochemistry analysis in **Supplementary Figure 2a**,**b**. T.U., N.G.F., M.J., K.N. and S. Akbarian contributed to the behavioral experiments in **Figure 2**. N.G.F. and J.D.R. wrote the manuscript. All authors contributed to interpretation and discussion of results and to editing of the manuscript.

COMPETING FINANCIAL INTERESTS

The authors declare no competing financial interests.

1. Penagarikano, O., Mulle, J.G. & Warren, S.T. *Annu. Rev. Genomics Hum. Genet.* **8**, 109–129 (2007).
2. Santoro, M.R., Bray, S.M. & Warren, S.T. *Annu. Rev. Pathol.* **7**, 219–245 (2012).
3. Verkerk, A.J. *et al. Cell* **65**, 905–914 (1991).
4. Feng, Y. *et al. J. Neurosci.* **17**, 1539–1547 (1997).
5. Darnell, J.C. *et al. Cell* **146**, 247–261 (2011).
6. Bear, M.F., Huber, K.M. & Warren, S.T. *Trends Neurosci.* **27**, 370–377 (2004).
7. Dölen, G. *et al. Neuron* **56**, 955–962 (2007).
8. Bassell, G.J. & Warren, S.T. *Neuron* **60**, 201–214 (2008).
9. Bhattacharya, A. *et al. Neuron* **76**, 325–337 (2012).
10. Qin, M., Kang, J., Burlin, T.V., Jiang, C. & Smith, C.B. *J. Neurosci.* **25**, 5087–5095 (2005).
11. Osterweil, E.K., Krueger, D.D., Reinhold, K. & Bear, M.F. *J. Neurosci.* **30**, 15616–15627 (2010).
12. Huber, K.M., Kayser, M.S. & Bear, M.F. *Science* **288**, 1254–1257 (2000).
13. Wu, L. *et al. Neuron* **21**, 1129–1139 (1998).
14. Huang, Y., Yario, T.A. & Steitz, J.A. *Proc. Natl. Acad. Sci. USA* **101**, 9666–9670 (2004).
15. Alarcon, J.M. *et al. Learn. Mem.* **11**, 318–327 (2004).
16. Zearfoss, N.R., Alarcon, J.M., Trifilieff, P., Kandel, E. & Richter, J.D. *J. Neurosci.* **28**, 8502–8509 (2008).
17. Huang, Y.S., Jung, M.Y., Sarkissian, M. & Richter, J.D. *EMBO J.* **21**, 2139–2148 (2002).
18. Udagawa, T. *et al. Mol. Cell* **47**, 253–266 (2012).
19. Berger-Sweeney, J., Zearfoss, N.R. & Richter, J.D. *Learn. Mem.* **13**, 4–7 (2006).
20. Auerbach, B.D., Osterweil, E.K. & Bear, M.F. *Nature* **480**, 63–68 (2011).
21. Shang, Y. *et al. J. Neurochem.* **111**, 635–646 (2009).
22. Pfeiffer, B.E. & Huber, K.M. *J. Neurosci.* **27**, 3120–3130 (2007).
23. Avgustinovich, D.F., Lipina, T.V., Bondar, N.P., Alekseyenko, O.V. & Kudryavtseva, N.N. *Behav. Genet.* **30**, 101–109 (2000).
24. Moretti, P., Bouwknecht, J.A., Teague, R., Paylor, R. & Zoghbi, H.Y. *Hum. Mol. Genet.* **14**, 205–220 (2005).
25. Laroche, S., Davis, S. & Jay, T.M. *Hippocampus* **10**, 438–446 (2000).
26. Lynch, M.A. *Physiol. Rev.* **84**, 87–136 (2004).
27. Feng, Y. *et al. Mol. Cell* **1**, 109–118 (1997).
28. Richter, J.D., Wasserman, W.J. & Smith, L.D. *Dev. Biol.* **89**, 159–167 (1982).
29. Santini, E. *et al. Nature* **493**, 411–415 (2013).
30. Gkogkas, C.G. *et al. Nature* **493**, 371–377 (2013).
31. Deacon, R.M.J. *Nat. Protoc.* **1**, 1117–1119 (2006).

ONLINE METHODS

Animals. All mice (C57BL/6) were maintained in a temperature- (25 °C), humidity- (50–60%) and light-controlled (12-h light-dark cycle) and pathogen-free environment. Animal protocols were approved for use by the University of Massachusetts Medical School Institutional Animal Care and Use Committee (IACUC).

Biochemical analyses and western blotting. Co-immunoprecipitations were performed using mouse brains or Neuro2A cells transfected with pcDNA-CPEB-HA as described[18]. Mouse monoclonal anti-HA (Covance, 16B12) and rabbit polyclonal anti-FMRP (Abcam, ab17722) antibodies were used for immunoprecipitation (2 µl of stock antibody). For western blot analysis, the hippocampus was rapidly dissected on ice from P28–P35 male mice of the indicated genotypes (**Supplementary Table 2**), rinsed briefly in 1× HBSS, then rapidly lysed in ice-cold lysis buffer (in mM: 10 HEPES pH 7.4, 2 EDTA, 2 EGTA, plus 1% Triton X-100, with protease (Roche) and phosphatase (CalBiochem) inhibitors). Samples were quantified by Coomassie Protein Assay (ThermoFisher), and 10 µg of sample was loaded per lane onto 6% or 12% Tris-glycine SDS-PAGE gels, transferred to PVDF and blotted with the antibodies indicated in **Supplementary Table 6**.

Slice labeling. Metabolic labeling experiments were performed as described previously[11], except as noted below. Briefly, 500-µm-thick hippocampal slices were prepared from P28–P30 male WT, *Fmr1* KO, *Cpeb1* KO and DKO mice. Littermate pairing was not possible given the genotype yield of the genetic crosses used, so mice were age matched as nearly as possible for all experiments. Slices recovered in artificial cerebrospinal fluid (ACFS, in mM: 125 NaCl, 2.5 KCl, 2 $CaCl_2$, 1 $MgCl_2$, 26 $NaHCO_3$, 1.25 NaH_2PO_4, 10 glucose, saturated with 95% CO_2 and 5% O_2) at 32 °C for 2.5 to 3.5 h before labeling. Slices were incubated in 25 µM actinomycin D (Sigma Aldrich) for 30 min, followed by 30 min of labeling in 10 µCi/mL [^{35}S]methionine labeling mix (PerkinElmer) in ACSF. After labeling, slices were snap frozen in liquid nitrogen. Slices were thawed for processing in ice-cold homogenization buffer (HB: 10 mM HEPES pH 7.4, 2 mM EDTA, 2 mM EGTA) containing protease (Roche) and phosphatase inhibitors (EMD Biosciences). Slices were then dounce homogenized in HB plus 1% Triton X-100. Proteins were precipitated with 10% trichloroacetic acid (TCA) on ice for 10 min. Protein pellets were resuspended in 1 N NaOH and then neutralized with HCl before aliquots were taken for scintillation counting and protein concentration assays. Radioactivity, as expressed in counts per minute per µg of protein, were normalized to the incorporation of the WT animal for each experiment.

Long-term depression analysis. Brains from mice 6–7 weeks of age with the indicated genotypes (**Fig. 1c**,**d**) were quickly removed and placed in ice-cold cutting solution (CS) composed of (in mM) 110 sucrose, 60 NaCl, 3 KCl, 1.25 NaH_2PO_4, 28 $NaHCO_3$, 0.5 $CaCl_2$, 7 $MgCl_2$, 5 D-glucose, and 0.6 ascorbate. Transverse hippocampal slices (400 µm) were prepared using a Leica VT1200 Vibratome (Leica, Bannockburn, IL). The slices were allowed to recover for 30 min at room temperature in 50:50 CS:ACSF, followed by additional recovery for 30 min in room-temperature ACSF.

After initial recovery, the slices were placed in an interface chamber (Scientific Systems Design, Mississauga, Ontario, Canada) and maintained at 32 °C in ACSF (2 mL/min). The slices were allowed to recover for an additional 120 min on the electrophysiology rig before experimentation. All solutions were constantly aerated with 95% O_2 + 5% CO_2. Bipolar stimulating electrodes (92:8 Pt:Y) were placed at the border of area CA3 and area CA1 along the Schaffer-Collateral pathway. ACSF-filled glass recording electrodes (1–3 MΩ) were placed in the stratum radiatum of area CA1. Basal synaptic transmission was assessed for each slice by applying gradually increasing stimuli (0.5–15 V), using a stimulus isolator (A-M Systems, Carlsborg, WA) and determining the input-output relationship. All subsequent stimuli applied to slices were equivalent to the level necessary to evoke a fEPSP that was 50% of the maximal initial slope that could be evoked. Synaptic efficacy was continuously monitored (0.05 Hz), and sweeps were averaged together every 2 min. fEPSPs were amplified (A-M Systems Model 1800) and digitized (Digidata 1440, Molecular Devices, Sunnyvale, CA) before analysis (pClamp, Molecular Devices, Sunnyvale, CA). A stable baseline synaptic transmission was established for at least 20 min. Once a stable baseline was established, the slices were treated with DHPG (50 µM) to induce long-term depression (LTD). The initial slopes of the fEPSPs from averaged traces were normalized to those obtained during the baseline recording. In some of the experiments, anisomycin (20 µM) was applied in the perfused ACSF for 20 min before, during and 30 min after the application of DHPG (50 µM).

Long-term potentiation analysis. Transverse hippocampal slices (400 µm) were obtained from adult (2.5–5 months old) mice. All procedures were performed in compliance with the Institutional Animal Care and Use Committee of the State University of New York, Downstate Medical Center. Slices were cut in ice-cold artificial cerebrospinal fluid (ACSF containing (in mM) 119 NaCl, 4.0 KCl, 1.5 $MgSO_4$, 2.5 $CaCl_2$, 26.2 $NaHCO_3$, 1 NaH_2PO_4 and 11 glucose saturated with 95% O_2, 5% CO_2) and then warmed in oxygenated ACSF to 35 °C for 45 min. Slices were thereafter allowed to equilibrate for at least 60 min in oxygenated ACSF at room temperature. For experiments, slices were immersed in a submerged recording chamber subfused with oxygenated ACSF at 35–36 °C. Field excitatory postsynaptic potentials (fEPSPs) from the dentate gyrus (DG) area were obtained via stimulation with bipolar electrodes (FHC & Co, ME, USA) and recording with borosilicate glass pipettes (5–10 mΩ) filled with ACSF solution. Responses from Schaffer collateral to CA1 cell synapses were obtained with a pair of stimulation and recording electrodes located in CA1 stratum radiatum. Test pulse intensity was set at approximately 40% of the maximum fEPSP slope. Test sampling was 0.017 Hz (once per minute), and test pulse duration was 50 µs. LTP was induced by theta burst stimulation (TBS): three bursts spaced by 20 s, each burst consisting of six trains of high-frequency stimulus (six pulses at 100 Hz) delivered at 10 Hz.

Spine density analysis. Spines on primary apical dendrites of hippocampal CA1 pyramidal neurons were analyzed using the Golgi-Cox method as described previously[32]. In this study, an apical dendrite originating directly from the cell soma was classified as the main shaft, and any branch arising from the main shaft is considered as the apical dendrite. Apical dendrites originating within 50–150 µm of the cell soma were chosen for spine-density analysis. By using the NeuroLucida system (100×, 1.3 numerical aperture, Olympus BX61), all protrusions, irrespective of their morphological characteristics, were counted as spines if they were in direct continuity with the main shaft. Spines were counted for a length of 60 µm. This total length of 60 µm was further subjected to a detailed segmental analysis, which consisted of counting the number of spines in successive steps of 10 µm each, for a total of six steps. Values for the number of spines from each 10-µm segment, at a given distance from the origin of the branch, were then averaged across all neurons in a particular experimental group.

Neuron culture and immunocytochemistry. For CPEB and FMRP co-localization experiments, primary hippocampal neurons were cultured from embryonic day 18 rat embryos as described[33]. For immunofluorescence, cultured hippocampal neurons (14–21 d *in vitro*) were fixed in 4% PFA and processed with mouse anti-FMRP (Millipore, IC3/MAB2160) together with rabbit anti-CPEB1 (ABR reagents, 13301) or rabbit anti-ZBP1 (G.J.B.'s laboratory) or rabbit anti-CPSF (J.D.L.'s laboratory). All primary antibodies were used at a dilution of 1:1,000. Neurons were imaged by wide-field epifluorescence microscopy with 60× oil objective on a Nikon TE Eclipse inverted microscope equipped with a motorized stage. Optical sections were captured at an interval of 0.15 µm using IP lab acquisition software. Image analysis was performed using Imaris (Bitplane) 3D Coloc module. A focused stack of five slices were subjected to quantification of co-localization by iterative randomization of one channel and co-localizing it with another to obtain an 'auto threshold', above which true co-localization was observed. To normalize dendrites from multiple neurons in the same experiment, a 'common threshold' above the autothreshold of all dendrites was chosen for each channel; the co-localization of all dendrites at which was used get an average percentage co-localization for the experiment. For *in vitro* synapse formation analysis, hippocampal or cortical neurons were cultured and synapsin staining was performed as described[22]. Neurons were imaged on a Nikon E600 Eclipse inverted fluorescence microscope equipped with a Model 18.2 color digital camera and SPOT software (Diagnostic Instruments). Images were analyzed using ImageJ.

doi:10.1038/nm.3353

Ribosome transit rate assay. The brain was rapidly removed from P28–P35 mice, rinsed in ice-cold 1× HBSS + 10 mM HEPES-KOH, rapidly dissected on ice to remove the cerebellum and midbrain (subsequently discarded), and the remaining tissue homogenized in 1 mL lysis buffer[34] (25 mM HEPES-KOH pH 7.4, 50 mM KCl, 1.5 mM $MgCl_2$, 0.5 mM DTT, plus EDTA-free protease inhibitor tablet (Roche) and 40 U/mL RNAse OUT (Invitrogen/Life Technologies), in a 2-mL glass dounce homogenizer, 20 strokes loose, 20 strokes tight), and centrifuged at low speed (2000*g* 10 min) to pellet insoluble material. To the resulting supernatant we added a creatine-based ATP regenerating mix (in mM: 125 HEPES-KOH pH 7.4, 10 ATP, 2 GTP, 100 creatine phosphate, 2 spermidine, plus 1 mg/mL creatine phosphokinase), 0.2 mM amino acids (without cysteine and methionine) and [^{35}S]methionine and [^{35}S]cysteine. For control experiments, 2 µM hippuristanol was also added[35]. The lysate was then warmed to 30 °C and samples were taken at indicated time points for SDS-PAGE. ^{35}S-labeled amino acid incorporation was assessed by phosphorimaging of SDS-PAGE gels. The relative amount of phosphor signal at 60–100 kDa was quantified in each lane using Image J and plotted as a percentage of the maximum (40 min) time point.

Audiogenic seizure. Mice (P19–P21) were individually habituated in a behavioral chamber made of transparent plastic for 2 min and were subjected to acoustic stimulus (125 dB at 0.25 m) using a personal alarm (RadioShack, 49-1010) for 2 min. All assays were carried out between 4 p.m. and 6 p.m. Audiogenic seizure phenotypes consisting of sequential responses of wild running, seizure and status epilepticus, or death, were noted.

T maze. This test was used to measure working memory performance in rodents[36,37]. The maze consisted of three equally sized arms (30 cm × 7.5 cm × 30 cm high) made from white plastic: one start arm leading in a 90° angle to the two target arms (opposing each other). All arms were equipped with sliding doors. During the test, mice were first confined in the start arm. Once the door of this arm was opened, the mouse was allowed to choose one of the target arms. The door of the opposing target arm was closed until the mouse returned to the start arm. The protocol was repeated until the mouse had made 15 choices. Additionally, the time that a mouse needed to complete this task was measured. To analyze working memory performance, the number of alternations between the target arms were counted.

Open-field test. This test was used to measure locomotor activity and anxiety in mice[23,38,39]. The apparatus consisted of an arena (40 cm × 40 cm) surrounded by 30-cm-high walls made of white plastic. The arena was illuminated with white light (350 lx). Mice were individually placed into the arena and allowed to explore the arena for 15 min. The total distance moved, indicative of locomotor activity, and the time spent in a virtual center (15 cm × 15 cm) of the open field to evaluate anxiety related behavior were determined. Behavior of the mice was tracked with the video-based EthoVision system (Noldus, Wageningen, The Netherlands).

Passive avoidance test. To measure long-term memory, a passive avoidance paradigm was employed[40–42]. The experiments were performed in a two-chamber passive avoidance box (Gemini, San Diego Instruments, San Diego, CA). Both boxes were equipped with a steel rod floor (20.5 cm × 25 cm surface) and interconnected by a sliding door. One box was not illuminated (≤10 lx) and the other box was illuminated with white light (250 lx). Mice were placed in the light compartment and left there for 1 min; the door separating the two compartments was then opened and the latency to enter the dark compartment was determined. The door was then closed and the mice received a foot shock (1 s, 0.25 mA); they were returned thereafter to their home cage. The same procedure was repeated 24 h later, but in the absence of a foot shock.

Home cage activity. Mice were individually housed for at least 3 d in a standard macrolon mouse cage (18 cm × 29 cm, 12 cm high) to ensure that they would perceive the cage as their home cage. They were then placed with their home cage into one frame of a photobeam activity system for home cage (San Diego Instruments, San Diego, CA). Activity was measured continuously for 24 h. For visual representation, the locomotor activity data for each hour were summarized.

Nesting assay. Nest building was assessed essentially as previously described[31] with the following changes: animals were single-housed with a 2.5-g nestlet and left undisturbed for 72 h. Nests were assessed and unused nestlet weighed, then a fresh nestlet was placed in the cage. A second assessment was performed 24 h later.

Bilateral hippocampal injection. To deliver *Cpeb1* shRNA into the dorsal hippocampus, P39–P44 *Fmr1* KO mice were anesthetized with a ketamine (100 mg/kg)/xylazine (10 mg/kg) mixture administered intraperitoneally and thereafter placed on a stereotactic frame (Stoelting) equipped with a mouse adaptor. Bilateral injection coordinates according to the mouse brain atlas[43] were (from bregma) −1.5 mm anteroposterior (AP), ± 1 mm mediolateral (ML) and 1.5 mm dorsoventral (DV). A 10-µl Hamilton syringe was used to inject 1 µL (0.25 µL/min) of PBS containing sh-Cpeb-GFP or control packaged lentivirus per hemisphere. shRNA plasmids and lentivirus were prepared as described[18]. After each injection, the syringe was left in place for 4 min to prevent backflow. Ten days after surgery, mice were tested in the T maze. After completion of the tests, brains were dissected and the knockdown efficacy of GFP-containing tissue was determined by quantitative RT-PCR. Based on previous hippocampal injections with lentivirus, we estimate approximately 50% of cells in the GFP-containing region of the brain were infected[18].

Statistical analyses. LTD data were analyzed by two-way repeated-measures ANOVA analysis. LTP data were analyzed with a two-way repeated-measures ANOVA test followed by a *post hoc* analysis for three independent populations between series of control and knockout groups (SigmaStat 3.5; Systat Software Inc., Germany). Spine density was analyzed by one-way ANOVA. Behavioral data were analyzed with the two-way ANOVA followed by *post hoc* analysis when appropriate. In cases where the data were not normally distributed as determined by Levene's test, they were analyzed with the non-parametric Mann-Whitney test. Western blot data were analyzed by Student's *t* test (WT versus respective genotype). In all cases, the determination of statistical significance was set to $P < 0.05$.

Bioinformatic identification of CPEB targets. To identify putative CPEB target mRNAs, mouse Refseq gene annotations of FMRP-CLIP targets[5] were downloaded from UCSC and processed to define their 3′ UTR coordinates. Of the 842 FMRP-CLIP targets, 827 were found to have annotated Refseq 3′ UTRs. The corresponding genomic sequences (mm9) of these regions were then searched for the presence of CPEs UUUUAAU and UUUUAU. An FMRP target containing one or more of these motifs within its terminal nucleotides (up to 300 nucleotides upstream of the annotated transcription end) was considered a potential CPEB target. Generally, this placed the CPE within 200–250 nucleotides from the cleavage and polyadenylation signal (AAUAAA)[44].

32. Raju, R.T. & Rao, B.S.S. *Brain and Behavior* 108–111 (National Institute of Mental Health and Neurosciences, Bangalore, India, 2004).
33. Antar, L.N., Afroz, R., Dictenberg, J.B., Carroll, R.C. & Bassell, G.J. *J. Neurosci.* **24**, 2648–2655 (2004).
34. Svitkin, Y.V. & Sonenberg, N. *Methods Enzymol.* **429**, 53–82 (2007).
35. Bordeleau, M.-E. *et al. Nat. Chem. Biol.* **2**, 213–220 (2006).
36. Deacon, R.M.J. & Rawlins, J.N.P. *Nat. Protoc.* **1**, 7–12 (2006).
37. Brito, L.S., Yamasaki, E.N., Paumgartten, F.J. & Brito, G.N. *Braz. J. Med. Biol. Res.* **20**, 125–135 (1987).
38. Engin, E. & Treit, D. *Behav. Pharmacol.* **18**, 365–374 (2007).
39. Ramos, A. & Mormede, P. *Neurosci. Biobehav. Rev.* **22**, 33–57 (1998).
40. Baarendse, P.J.J. *et al. Hippocampus* **18**, 11–19 (2008).
41. Morellini, F. & Schachner, M. *Eur. J. Neurosci.* **23**, 1255–1268 (2006).
42. Morellini, F. *et al. Cereb. Cortex* **20**, 2712–2727 (2010).
43. Paxinos, G. & Franklin, K.B.J. *The Mouse Brain in Stereotaxic Coordinates* (Academic Press, 2001).
44. McGrew, L.L. & Richter, J.D. *EMBO J.* **9**, 3743–3751 (1990).